Manipulating and probing the growth of plasmonic nanoparticle arrays using light

Oral Ualibek,[a] Ruggero Verre,*[a] Brendan Bulfin,[a] Victor Usov,[a] Karsten Fleischer,[a,b] John F. McGilp[b] and Igor V. Shvets[a,b]

Received Xth XXXXXXXXXX 20XX, Accepted Xth XXXXXXXXX 20XX
First published on the web Xth XXXXXXXXXX 200X
DOI: 10.1039/b000000x

Highly ordered self-assembled silver nanoparticle (NP) arrays have been produced by glancing angle deposition on faceted c-plane Al_2O_3 templates. The NP shape can be tuned by changing the substrate temperature during deposition. Reflectance anisotropy spectroscopy has been used to monitor the plasmonic evolution of the sample during the growth. The structures showed a strong dichroic response related to NP anisotropy and dipolar coupling. Furthermore, multipolar resonances due to sharp edge effects between NP and substrate were observed. Analytical and numerical methods have been used to explain the results and extract semi-quantitative information on the morphology of the NPs. The results provide insight on the growth mechanisms by the glancing angle deposition. Finally, it has been shown that the NP morphology can be manipulated by a simple illumination the surface with an intense light source, inducing changes in the optical response. This opens up new possibilities for engineering plasmonic structure over large active areas.

1 Introduction

Metal nanoparticles (NPs) have attracted a significant scientific attention in the last decade.[1,2] In particular, localised plasmon resonance (LPR) effects have provided substantial advantages in many fields such as biological analysis by enhanced luminescence or Raman scattering[3,4] and optical circuits.[5] A wide range of applications is possible as the plasmonic properties of metal NPs can be tuned by changing their size and shape.[6] Particular interest has been focused in the area of coupled NPs[7,8] as they provide more flexibility and advanced functionalities. Coupled NP arrays have been used as building blocks for wave guides[9–11] and to increase solar cell efficiency.[12–14] Furthermore, the local electric field enhancement in the gap region between closely spaced NPs has been utilised in surface enhanced Raman spectroscopy,[15] second harmonic generation,[16] enhanced fluorescence[17] and optical tweezers.[18] The majority of these devices are based on planar geometries, preferably with NPs uniformly dispersed over large areas.

Different methods have been developed to produce metallic NP arrays, but many challenges remain. For instance, lithographic methods cannot be sufficiently up-scaled while colloidal methods result in randomly distributed NPs.[19] Recently, we developed a different fabrication method based on deposition at glancing angle on a stepped template.[20–24] Adatoms are evaporated towards a stepped template surface at shallow angles of incidence. The step edge shadows part of the surface during the deposition and highly ordered NPs are created by self-assembly on the step edge. The principle, often refered to as glancing angle deposition (GLAD)[25,26], is simple and is mainly based on geometrical considerations, rendering it largely independent of the deposited material in the case of step shadowing.[27]

Whenever NPs are deposited onto a substrate an accurate control of the parameters governing the growth is important for tailoring the resulting NP morphology and for growth reproducibility. Material properties, substrate temperature,[28] adatom flux,[29] pressure and the direction of the adatoms plume towards the substrate[30] play a crucial role in the growth. Changes in one or several parameters results in a modified plasmonic response due to changes in the NP morphology. However, the effect of each individual parameter is difficult to separate from the others. In order for such a self-assembled production method to be competitive, the effect of each of the deposition parameter on the growth condition needs to be well understood and controlled.

One solution is real time monitoring of optical properties of the system as it is being fabricated. This provides information on the growth mechanism and allows production of structures with the desired optical characteristics. In the case of physical vapour depositions this route is complicated as the growth is usually performed in a vacuum environment. Different optical methods, such as spectroscopic ellipsometry,[31–33] polarized reflectivity[28] and reflectance anisotropy spectroscopy (RAS)[23] have been used for monitoring the growth evolution.

[a] *Centre for Research on Adaptive Nanostructures and Nanodevices (CRANN), School of Physics, Trinity College Dublin, Dublin 2 , Ireland*
[b] *School of Physics, Trinity College Dublin, Dublin 2 , Ireland*

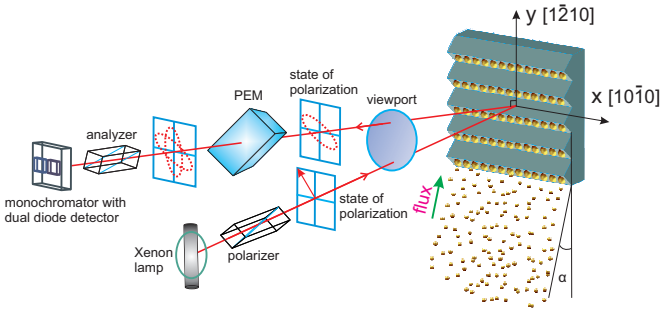

Fig. 1 Schematic set-up for the *in-situ* RAS measurements during glancing angle deposition. The stepped surface is oriented to allow for measurements of the anisotropy and simultaneous deposition at a glancing angle α.

We have recently utilised RAS to measure *in situ* the optical response of NP arrays grown by glancing angle deposition.[24] Figure 1 illustrates the configuration used by us. The sample is placed in an UHV environment, facing a low-strain view port to allow for the RAS measurement at near normal incidence. The template is oriented with horizontal steps and slightly tilted to allow for a glancing angle ($\alpha\sim6°$) deposition from a Knudsen cell at the bottom of the chamber.

RAS in general is a reflection based measurement. It probes the difference in the complex Fresnel reflection coefficients of the whole sample ($\Delta\tilde{r}$) at near normal incidence between two orthogonal directions in the surface plane (x, y), normalized to the mean value ($\tilde{r}$):[34,35]

$$\frac{\Delta\tilde{r}}{\tilde{r}} = \frac{2(\tilde{r}_x - \tilde{r}_y)}{\tilde{r}_x + \tilde{r}_y}. \qquad (1)$$

As the RAS signal for an isotropic substrate is zero, the measured signal only arises from anisotropic regions in the sample, in our case the plasmonic structures, and is therefore more sensitive than absolute measurements of the samples reflectivity. The technique measures the complete expression (1) directly, not the individual components $\tilde{r}_i$ and due to the inherent self-normalisation by the total reflectance is very stable in terms of sample misalignment, background lighting and spectral shape of the light source, which makes it ideally suited for *in-situ* monitoring.[35,36]

In this manuscript RAS will be used to extract information on the growth mechanisms of NP arrays. As the NP optical response is measured directly in a vacuum environment no tarnishing or oxidation takes place and the exact origin of the optical resonances can be determined. The *in-situ* measurement also allows for tailoring of the NP morphology by changing the deposition parameters. Numerical and analytical calculations will be compared with the experiment, and the optical features related with the equilibrium NP morphology will be explained using surface free energy considerations. The analysis of the plasmonic response provides clear insight on the growth evolution, which cannot be easily addressed by any other characterization method. In particular the numerical simulations make it possible to discuss the effects of NP coupling, image charge and the sharpness of the edge at the interface between NP and substrate in greater detail.

The effect of varying the substrate temperature during deposition will be analysed as a convenient route to manipulate the morphology of the NPs. Finally we will demonstrate that illuminating the NP arrays with intense visible light the NPs undergo a significant change in their shape and distribution on the surface due to localised heating of the deposited material. This effect can be described as direct plasmon manipulation[37] and can be easily utilised to modify the plasmonic response over a large, illuminated area.[38]

2 Experiment

Silver NP arrays were grown onto a stepped α-Al_2O_3 substrate. Single crystal, single side polished c-plane α-Al_2O_3 (MTI K.J group, USA) off-cut towards the [1$\bar{2}$10] direction by 6°were used. The sample was treated in an ultrasonic bath using acetone, methanol and high purity isopropanol and loaded in a high temperature tube furnace. The sample was then annealed at temperature 1410°C for 24 hours and investigated using an Asyluum research atomic force microscope. The surface is composed of periodic alternating facets with a period of 80±15 nm, in accordance with previous studies.[39,40]

The faceted template was cut into 4 square pieces using a diamond saw. This allowed arrays grown on identical templates under different deposition parameters to be compared. Each piece was sonicated and mounted in an ultra high vacuum (UHV) chamber.[41] The sample surface was tilted at a glancing angle of α=6° with respect to the adatom flux. This deposition angle was previously demonstrated to provide the most ordered NP arrangement.[23] Silver was deposited at a pressure of 4×10^{-8} mbar and a constant adatom flux Φ at normal incidence (α=90°) of 2.5 Å/min. The deposition time t was kept constant at 30 minutes for all samples. Due to the inclination of the sample within the flux, the nominal thickness T of the deposited material is much lower according to

$$T = t \times \Phi \times \sin\alpha. \qquad (2)$$

This nominal thickness is proportional to the actual amount of deposited material. Due to the effect of shadowing and the reorganisation of the material into the NPs the actual height of the NP (Z_{NP}) will be higher.

During the deposition the substrate was kept at different temperatures of 20°C (RT), 100°C, 200°C and 300°C. The temperature was previously calibrated using a reference thermocouple with a sample surface temperature error of ±5°.

RAS spectra were recorded during growth interruptions and, later, after exposure of the sample to atmosphere.

The RAS system is a home built system, following the two polariser, photoelastic modulator design.[34] The x and y indexes in Eq. (1) refer to the in-plane directions along and perpendicular to the steps/NP array respectively (see Fig. 1).

To extract exact information about NP dimensions and separations the surface was finally imaged using an ULTRA scanning electron microscope (SEM) by C. Zeiss. SEM images were analysed using AutoCAD scripts to extract typical dimensions such as NP diameter D, ellipticity s or spacing L. At least 1000 NPs imaged over different areas were used to accumulate statistics.

In a final experiment the sample deposited at room temperature was subsequently illuminated by focused light from a Xe lamp. Illumination was carried out in a separate chamber purged with N_2. The sample was annealed for 90 seconds, the power of the beam was 40 W/cm^2 and the illuminated area $\sim$1 cm^2. After annealing, the sample was scanned once again with SEM and the optical properties were measured by RAS.

Previous analytical models of the anisotropic optical response have succesfully described the plasmonic response of NP arrays.[23,27] However certain aspects such as quadrupolar resonances, estimations of the electrical field distribution between the NPs, or the influence of the NP shape (sperical, hemispherical, truncated spheres) can not be investigated by simple analytical models. For a more general approach, numerical simulations were performed using the finite element method (FEM) COMSOL multiphysics package. NPs enclosed within a box segmented into 28000 tetrahedral elements was calculated. The mesh was distributed so that the elements were approximately four times denser in the close vicinity of the nano particles than they were at the extremities of the bounding box. For a mesh of this density no noticeable change in the solution was seen by further increasing the mesh. The model was solved in stationary state with periodic boundary conditions at the side walls of the box (physically equivalent to an infinite array in the x and y direction). The upper boundary was set to be the incoming light at normal incidence. The light was allowed to escape from the bottom boundary by setting another scattering boundary condition. The FEM simulation used the bulk Ag dielectric function with a correction in the IR free electron response to take into account the reduced dimensions of the NPs.[42,43] The reflectance R_i for light polarised along a given direction i=(x,y) was assumed to be proportional to the intensity of light exiting the top surface. A reflectance anisotropy $\Delta R/R = 2(R_x - R_y)/(R_x + R_y)$ can than be calculated. As the reflectance is linked to the complex Fresnel reflectivity of a sample as $R_i = |\tilde{r}_i|^2$ one can directly compared these simulated RAS spectra to measurements: $\Delta R/R \approx 2\mathrm{Re}[\Delta\tilde{r}/\tilde{r}]$. However, due to small scaling differences caused by the size distribution in real samples when compared to ideal modelled structures, only normalised spectra will be compared in this article.

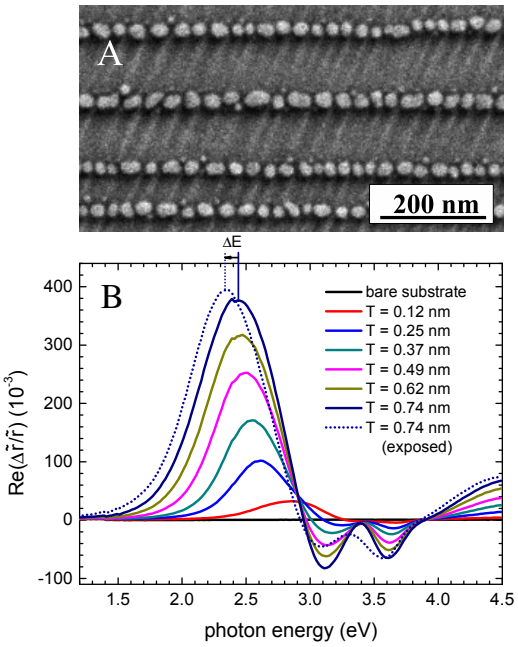

Fig. 2 (A) SEM image of the Ag NP arrays grown on a faceted c-plane Al_2O_3 substrate at room temperature. (B) Evolution of the RAS spectra recorded during the growth. T is the nominal deposited thickness as defined in Eq. (2). The dotted spectra was recorded after exposure of the thickest sample to air

3 Experimental results

The morphology of the Ag NP array after deposition at RT is shown in Fig. 2A. The surface is covered by ordered NPs aligned along the facet and slightly elongated along the array direction. The morphology of NPs is consistent with a 3D cluster growth mechanism with a diffusion barrier between facet and terrace.[24] Due to the texturing of the template and the glancing angle of the flux, adatoms land on the facet only and NPs are formed as Ag does not wet the substrate. As the (0001) terraces also have the lowest surface free energy,[44] the adatoms cannot overcome the diffusion barrier between step and terraces and all the material distributes within the facets only.

The growth evolution was monitored using RAS *in-situ* and the results are shown in Fig. 2B. The bare substrate was measured to be isotropic, as expected for c-plane sapphire. Prominent features appear already for a nominal thickness T=0.1 nm. A positive peak develops around 2.5 eV and negative features are observed at higher energies. The positive

peak undergoes a red shift and the intensity of the peaks increases with increasing deposition time. The positive peaks red shift by an additional ΔE ~0.1-0.2 eV upon the exposure of the sample to the atmosphere and the negative features are smoothed. This behaviour is consistent with the formation of a thin Ag_2S layer covering the NP upon exposure of the sample to atmosphere.[24] It was previously demonstrated that for Ag NP arrays grown at glancing angle, RAS and polarized transmission spectroscopy provide equivalent information.[23] In particular, the strong positive peak describes the resonance along the NP array while the negative peaks arise from the in-plane resonance in the orthogonal direction. The additional negative features were assigned to quadrupolar resonances due to sharp edges.[45] The development of the RAS signal upon deposition can hence be explained: There is an initial nucleation of small, relatively wide spaced, weakly interacting NPs. For increasing thickness NPs get bigger and more regularly spaced, leading to the stronger amplitude of the RAS spectra, while the reduced spacing of the NP, as well as the growing ellipticity of the NPs lead to the red shift of positive peak.

The results confirm that ordered NP arrays can be produced at glancing angle, and that RAS can measure their optical properties during deposition. As the resonance position changes with the deposition time, in principle the growth could be stopped to produce structures with resonance peaks at the required energy.[27] However, the possibility of modifying the optical properties of the structures is limited by factors such as the diffusion constant of the adatoms or the material optical properties. We have previously developed a route to grow NP arrays with the desired optical response by changing the material of the NPs (Cu, Au or Ag) or the template periodicity. In this way the positive peak of the RAS spectrum can be positioned anywhere in the visible range.[27] However, modification of the deposition parameters also resulted in a decrease in the overall order of the structures. Consequently, broader plasmonic resonances occur, which potentially reduces the sensitivity of any optical biosensor based on refractive index changes around the NPs.

In the following we will show that varying the substrate temperature during deposition can improve the overall order of the NP distribution and can increase the tunable range of the resonance peak position. Fig. 3 shows the surface morphology for different substrate temperatures and the resulting RAS spectra before and after exposure of the sample to atmosphere. SEM images have been analysed to give the sample statistics shown in Table 1. The NP in-plane axis lengths D_i, the centre to centre distances L_i and the number of particles per unit area N at each substrate temperature are listed. The in-plane centre to centre distance L_x slightly decreases with increasing substrate temperature. Also the average major axis of the NP along the chain is decreased and the minor axis is almost constant, causing a decrease in the aspect ratio $s = D_x/D_y$ for

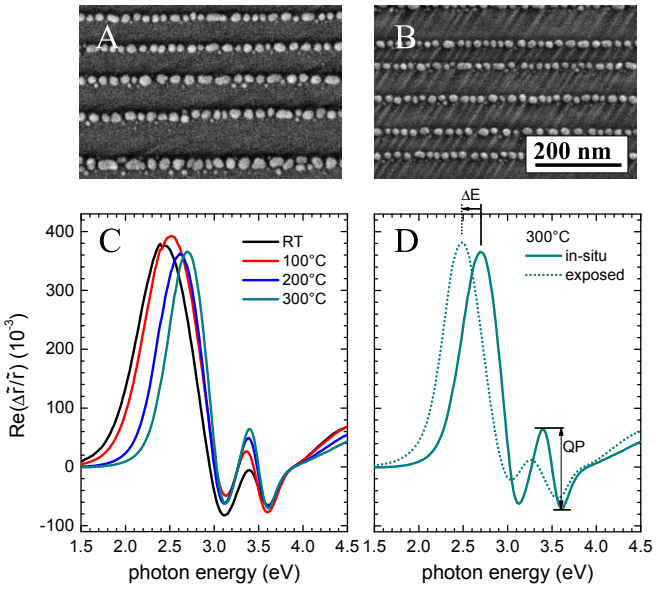

Fig. 3 SEM images of Ag NP arrays grown at 100 °C (A) and 300 °C (B). Deposition of Ag at higher temperature leads to more ordered and more spherical NPs. (C) RAS spectra after the deposition of nominally T=0.74 nm Ag NP. (D) compares the spectra of the sample grown at 300°C before and after exposure. A red shift ΔE for the positive resonance is observed, together with a smoothing of the quadrupolar features (QP).

increasing substrate temperature.

The changes can be explained using a simple diffusive picture. If Ag adatoms are deposited at room temperature, diffusion over the surface is limited. The seeds are formed at random positions, they grow and start merging together along the facets, resulting in elongated structures. Conversely, if the Ag is deposited at higher temperatures, adatom diffusion is increased and more ordered arrangements are obtained. The NP axis length perpendicular to the array (D_y) is almost constant due to the facet confinement, which explains the decrease in the NP aspect ratio at higher temperatures. Table 1 also shows that the NP size dispersion decreases at higher temperatures. The deposition time and angle was kept constant between samples, resulting in a consistent volume of deposited Ag (T=0.74 nm). The changes in the NP height (extracted from the optical model) are consistent with the expectation, as the average NP volume times number of NPs should also be constant.

Changes in the peak positions of the RAS spectra have been also observed (see Fig. 3C). Due to a decrease in the aspect ratio s of the NP and reduced NP interaction due to a bigger gap, the red shift of the positive resonance is reduced for samples grown at higher surface temperature, leading to an apparent blue shift of the structures compared to spectra from RT samples. Interestingly, the plasmonic resonance peaks be-

T (°C)	20	100	200	300
D_x (nm)	25 (10)	25 (11)	21 (7)	20 (7)
D_y (nm)	21 (6)	21 (7)	19 (5)	18 (5)
Z_{NP} (nm)	9 (1)	9 (1)	10 (1)	10.5 (1)
$s = d_x/d_y$	1.21	1.19	1.13	1.09
L_x (nm)	25 (11)	28 (13)	24 (10)	22 (10)
L_y (nm)	80 (15)	80 (15)	80 (15)	80 (15)
N/m^2 ($\times 10^{14}$)	4.9(2.3)	4.5 (2.2)	5.2 (2.4)	5.5 (2.7)

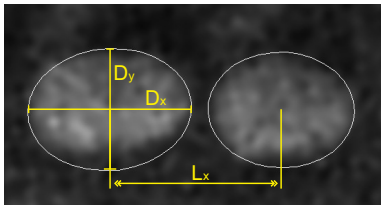

Table 1 Average morphology of Ag NP arrays as a function of the substrate temperature, with standard deviation in parenthesis. The average axis lengths D_i, the aspect ratio s, the centre to centre distance L_i and the number of particles per unit area N as extracted by the SEM images are reported. The x and y indexes are referred to the in-plane directions parallel and perpendicular to the array respectively. The nanoparticle height (Z_{NP}) values are obtained from the simulations of the optical spectra discussed in Section 4. The graph in the left shows a small part of an SEM image, indicating the fitted shape, and lengths for 2 NPs. Data in this table are derived from at least 1000 of such shape fits.

come sharper as the deposition temperature increases. This is expected, as the Gaussian broadening due to morphological dispersion decreases.[23] Reducing the size distribution is an important aspect, as it ensures higher sensitivity for any refractive index optical biosensor.[46] Finally the spectral feature at ∼3.4 eV increases in intensity and becomes positive at higher temperatures, but reduces in intensity on tarnishing by exposure to atmosphere. We attribute these structures to quadrupolar resonances, which will be affected by the shape of the NP edges, more dramatically than the dipolar resonances. To understand this behaviour was one of the main reasons to apply the numerical simulations outlined in the following.

4 Theory and discussion

The changes in the RAS spectrum discussed in the previous section will be now analysed in a semi-quantitative way and the dependency of the structure upon the various parameters involved in the simulation addressed.

First an analytical solution for the Ag NP arrays produced has been developed by us. The system has been modelled as an ensemble of identical ellipsoidal NPs supported on a substrate in a rectangular lattice. The Ag dielectric function was corrected in order to take into account the increase in the scattering rate at the particle surface. As the features of the nanocomposite layer are much smaller than the wavelength of the exciting light, the quasistatic approximation is used and only dipolar excitation modes can be considered.

The effective dielectric function of such a NP layer along the i-th direction is given by[47–49]

$$\bar{\varepsilon}_i = \varepsilon_{cap}(1 + \frac{N\alpha_i}{1 + \alpha_i\beta_i}). \qquad (3)$$

Equation (3) is based on a model, including the dielectric function of a capping layer describing a dielectric material ε_{cap} in the surrounding area of the NP. In order to take into consideration the presence of the steps, the NPs are assumed to be surrounded by a homogeneous medium composed of 30% alumina and 70% air.[24] α is the polarizability of the isolated NP[50] and β represents the anisotropic dipolar coupling between NPs. If the NP are considered identical and the image charges are taken into consideration[24]

$$\beta = \frac{1}{4\pi}\sum_{j\leq 10}(F\frac{3\cos^2\theta_j^{'} - 1}{r_j^{'3}} + \frac{3\cos^2\theta_j - 1}{r_j^3}), \qquad (4)$$

where θ and $\theta^{'}$ are the dipole and the image dipole angles respectively. The r_j ($r_j^{'}$) represents the distance between an ellipsoid centred in the origin and the j-th NP (or its image charge). The coefficient F in (4) is required to take into account the discontinuity between capping layer and substrate at the interface.[51,52] Once the anisotropic effective dielectric function is obtained, the in-plane complex reflection coefficients can be calculated using a transfer matrix formalism[53,54] and the RAS simulated by using (1).

Transfer matrix models and analytical expressions for a three layer model need a given optical thickness for the anisotropic dielectric medium. For thin films with a thickness $d \ll \lambda$, typically only the optical thickness $d\varepsilon$ can be analysed. In order to compare the simulated dielectric function ε of the NP layer with optical measurements we hence need to define the thickness of the layer. While related to the NP height Z_{NP} this is not equivalent to it, as for an inhomogeneous system as ours, the reflectivity of the uncovered terraces also contribute. To still be able to directly compare the measurements with the simulations we assume an effective thickness of the NP layer of d = 0.7 nm was used for all samples in line with the nominal thickness of a smooth layer if grown under the same conditions $t\Phi\sin\alpha$ =0.74 nm. While this is a crude estimation it resulted in calculated RAS amplitudes comparable to those measured.

To calculate the dielectric function of the NP layer, the measured parameters listed in Table 1 were used. Only one morphological parameter – the out-of-plane semi-axis, or NP

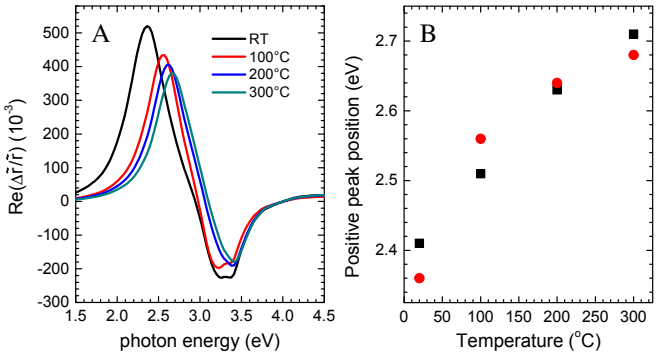

Fig. 4 (A) Simulated RAS spectra of the Ag NP arrays by using an analytical model. (B) Position of the positive RAS peak for the samples grown at different substrate temperatures. Both experiment (squares) and Theory (circles) are indicated.

height, Z_{NP} was treated as a fitting parameter. The fitted NP height of ≈9 nm was obtained under the constraint of a fixed overall Ag volume and is in agreement with the nominal thickness if we consider a filling factor of ≈ 0.09 as extracted from SEM analysis. The filling factor describes the area ratio between covered and uncovered areas. Fig. 4A shows the resulting spectra where the NP dielectric function has been scaled down by an additional 20% to take into consideration the broadening due to morphological dispersion. The simulation reproduces the shift in the positive peak position (see Fig. 4B) for different substrate temperatures. An analysis of the various parameters influencing the final spectral shape of the nanocomposite layer suggests the shifts in resonance position are related to an interplay between island anisotropy and NP dipolar coupling. More isotropic in-plane NPs and more separated NPs produce a blue shift of the original x resonance. However, as only dipolar resonances can be simulated with this analytical model, the negative peak appears as a single, sharp resonance present at higher energies than observed.

In order to investigate the origin of the additional features observed at higher energy, a FEM simulation has been performed. The analysis was simplified by assuming the NPs to be in-plane symmetric with $D_x = D_y = 22$ nm and a centre-to-centre distance of $L_x = 28$ nm and $L_y = 80$ nm. Any in-plane optical anisotropic response then arises from coupling between the NPs. The unit cell during the simulations consisted of a truncated Ag sphere resting on top of a transparent substrate with ε_{sub}=3.24 (similar to the dielectric function of single crystal Al_2O_3). The choice of truncated spheres was motivated by TEM images of such NPs[24], and the fact that we did observe strong deviations from the simple dipolar model. For sharp edges, such as the edges of truncated spheres, stronger quadrupolar resonances would be expected.

The simulations were performed by truncating a silver sphere in different positions. For convenience a parameter

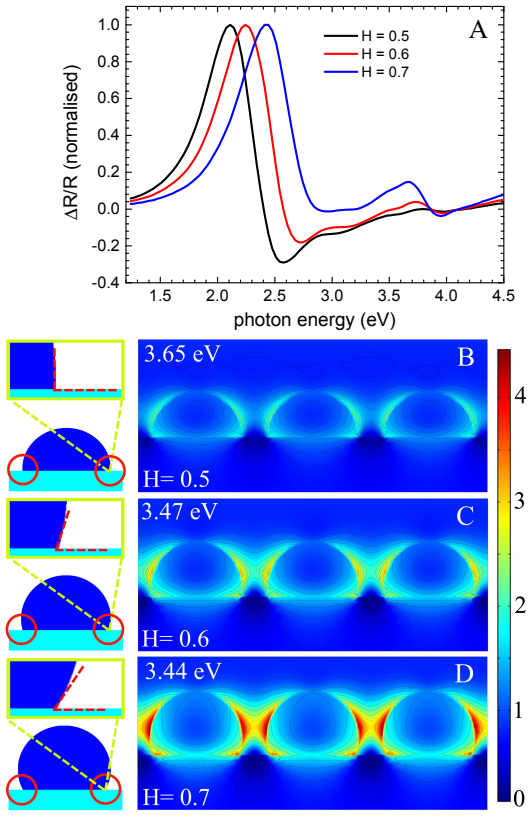

Fig. 5 (A) Normalised RAS spectra of truncated Ag spherical NP arrays simulated using FEM for different truncation positions. For extruding spheres (H = 0.7) a positive resonance is observable at high energy (∼3.5 eV). This resonance arises from quadrupolar excitation modes from the sharp edges between NPs and the substrate. Sections of the electric field mapping along the array at the quadrupolar resonance energy for different spherical truncations are shown in B, C, and D respectively. A normalised incident electric field E_0 =1 is assumed, and the same scale is used for all the images. A clear increase in the intensity of the electric field can be observed for the extruded NPs and it has been related with a decrease in the contact angle between substrate and NP (see sketches on the left).

H was defined as the ratio between the height of the truncated sphere to its in-plane diameter. The simulations were performed with H = 0.5 (truncated hemisphere), 0.6 and 0.7. The normalised simulated RAS spectra are shown in Fig. 5A. The positive feature at ∼3.5 eV appears in the RAS spectra for extruded NPs (H=0.7), similar to Fig. 3C. The increase in intensity as H increases can be explained by observing a section of the electric field mapping along the array at the quadrupolar resonance energy for different spherical truncations. A much greater enhancement of the local electric field is observed for the protruded NPs, particularly where the curvature is greatest in the contact region with the substrate. The more intense field

produces an increase in the resonance intensity at ∼3.5 eV. It can be seen that the blue shift of the positive resonance at ∼2.5 eV on increasing the substrate temperature (Fig. 3C) is also reproduced by the numerical simulation (Fig. 5A).

As the FEM simulation deals with truncated spheres rather than ellipsoids, the assignment of the features at ∼3.5 eV in Fig. 5C to quadrupolar effects appears reasonable. The analytic simulation finds an increase in NP height, together with a decrease in the lateral dimensions, as the substrate temperature is increased (Table 1). This is consistent with the evolution of NP shape represented schematically in Fig. 5. In addition, the decrease in intensity in this spectral region on exposure to atmosphere (Fig. 3D) can be explained by the reduction in curvature of the NPs on tarnishing. The FEM method suggests that the different quadrupolar intensities observed in the experiment are related to the different contact angles between the substrate and NP. This can be controlled via the substrate temperature as the final NP morphology is governed by surface energy considerations.

The substrate/air interface of Al_2O_3 has lower surface free energy than the substrate/Ag interface.[55] Therefore, the metal does not wet the surface and the contact area between NP and substrate tends to be minimised. This phenomenon is more pronounced at higher substrate temperatures when the adatoms have enough energy to rearrange on the substrate. The increase in the adatom mobility produces the extrusion from the surface to decrease the contact area. Such changes in the NP morphology have already been observed for different metals on oxide surfaces,[56] supporting this interpretation of the results. It is important to note that the sticking coefficient of Ag on Al_2O_3 does not vary significantly with the substrate temperature[56] and cannot explain the large changes in the in-plane morphology of the samples observed by micrograph analysis.

It has been shown that RAS provides a rich source of information on the morphology of the system. Firstly, it can measure resonance positions due to its *in situ* capability. The energy of the resonance is closely related to the morphological anisotropy of the system and to NP coupling. Secondly, it gives indication on the out-of-plane morphology of the NPs via the quadrupolar resonance intensity, also measured *in situ*. Finally, it has already been demonstrated that RAS readily provides information on the order of the system through the broadening of the positive resonances.[23]

5 Plasmon manipulation

In the previous sections it was shown that the final morphology can be tuned by varying the substrate temperature during the growth. The changes were ascribed to an increase in the adatom mobility, resulting in a different morphology of the NPs. Changing the morphology should also be possible

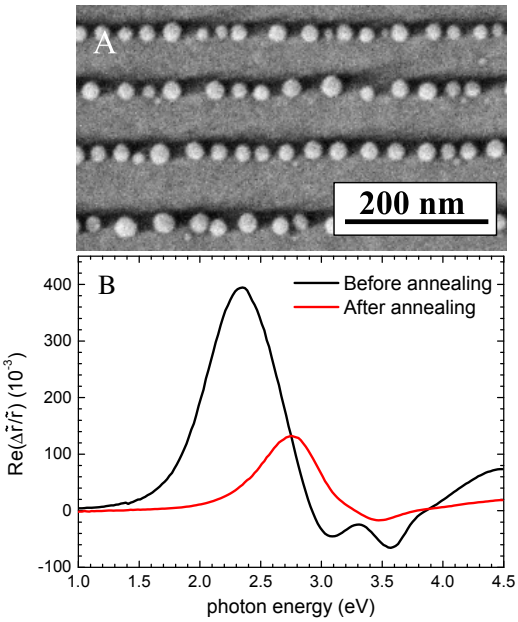

Fig. 6 (A) SEM images of the Ag NP arrays after the annealing using a Xe lamp. Exposure of the sample to intense focused light modifies the morphology of the NP arrays (cf. Fig. 2A). (B) RAS spectra of the Ag NP arrays before and after the annealing.

if the adatoms can be rendered mobile after deposition. This has been achieved by illuminating the surface using intense focused light. Such phenomena were discovered almost 20 years ago[57] and are known as plasmon manipulation.[37] The sample with NPs deposited at RT was illuminated by a Xe-lamp. Fig. 6A shows a SEM image of the surface after annealing. From a comparison with Fig. 2A it is evident that the NP morphology has been substantially modified. The NPs appear now in-plane spherical (D=26±4 nm) and the separation between the NPs is increased (L_x=33±8 nm). In our experiment the surface is illuminated by light with a homogeneous spectrum over the whole visible range. This leads to resonances in each NP and, due to the intense light source power, causes localised absorption and heating. The NPs melt and redistribute more homogeneously on the surface. As a result, the separation between NPs increases. As the NPs are polycrystalline[24] there is no preferential growth direction and NPs assume a spherical shape. It is interesting to note that the large changes in the morphology have been obtained using a Xe lamp and not, as previously utilised,[37] a focused Gaussian laser beam. This approach again allows easier up-scaling, as larger areas can be illuminated at once. As a broad band illumination source is utilised all NPs can undergo resonant absorption at the same time, even in samples with originally inhomogeneous NP size distribution. By illuminating specific areas of the device using distinct powers, one could also produce different responses

in the same device. Finally, the incidence power of the light source in the spectral region where we expect resonant absorption (1.8-2.8 eV) is $\sim$10 W/cm^2. Such a value is much smaller than that previously utilised to produce a migration of NPs on the surface.[58] The approach developed here therefore provides significant advantages compared to previously reported methods.

RAS spectra recorded before and after plasmon manipulation are shown in Fig. 6B. The resonance shifts towards the blue on annealing as a consequence of the more spherical character of the NP and an increase in the NP separation. Also, as the sample is more isotropic, the RAS amplitude decreases. Furthermore, since the annealing was done at atmospheric pressure, the NP is significantly tarnished, resulting in the complete disappearance of the quadrupolar features.

6 Conclusion

We have described how glancing angle deposition can produce highly ordered Ag NP arrays, and how RAS can monitor the changes in their optical behaviour *in situ*. It is demonstrated that tunability of the dipolar plasmonic resonances can be achieved by modifying the substrate temperature during annealing, where modification of the NP aspect ratio caused by an increase of the adatom diffusion on the faceted templates occur. Also, a higher energy resonance has been observed and related to a quadrupolar resonance associated with sharp edges between substrate and NPs, a conclusion supported by analytical and numerical modelling.

These results suggest a way to engineer the NP morphology by post-annealing of the sample and it was shown that this can be effectively achieved by exposing the surface to an intense broadband light source. This allows the NPs to be physically manipulated by external means over large active areas.

7 Acknowledgement

This work has been funded by Science Fundation of Ireland, Contract Nos 06/IN.1/I91and 11/RFP.1/PHY/3047, and conducted under the framework of the INSPIRE programme, funded by the Irish Government's Programme for Research in Third Level Institutions, Cycle 4, National Development Plan 2007-2013. O. Ualibek would like to acknowledge the support of the Government of republic of Kazakhstan under Bolashak programme.

References

1 S. A. Maier, *Plasmonics: Fundamentals and Applications*, Springer, 2007.

2 H. Chen, F. Wang, K. Li, K. C. Woo, J. Wang, Q. Li, L.-D. Sun, X. Zhang, H.-Q. Lin and C.-H. Yan, *ACS Nano*, 2012, **6**, 7162.

3 Y. H. Su, S.-L. Tu, S.-W. Tseng, Y.-C. Chang, S.-H. Chang and W.-M. Zhang, *Nanoscale*, 2010, **2**, 2639.

4 S. Nie and S. R. Emory, *Science*, 1997, **275**, 1102.

5 N. Engheta, *Science*, 2007, **317**, 1698.

6 U. Kreibig and M. Vollmer, *Optical Properties of Metal Clusters*, Springer, Berlin, 1957.

7 A. Bouhelier, R. Bachelot, J. S. Im, G. P. Wiederrecht, G. Lerondel, S. Kostcheev and P. Royer, *J. Phys. Chem. B*, 2005, **109**, 3195.

8 L. Shao, K. C. Woo, H. Chen, Z. Jin, J. Wang and H.-Q. Lin, *ACS Nano*, 2010, **4**, 3053.

9 M. Quinten, A. Leitner, J. R. Krenn and F. R. Aussenegg, *Opt. Lett.*, 1998, **23**, 1331.

10 B. Lamprecht, G. Schider, R. T. Lechner, H. Ditlbacher, J. R. Krenn, A. Leitner and F. R. Aussenegg, *Phys. Rev. Lett.*, 2000, **84**, 4721.

11 S. A. Maier, P. G. Kik, H. A. Atwater, S. Meltzer, E. Harel, B. E. Koel and A. Requicha, *Nat.Mater.*, 2003, **2**, 229.

12 G. Pellegrini, G. Mattei and P. Mazzoldi, *Nanotech.*, 2009, **20**, 065201.

13 H. A. Atwater and A. Polman, *Nat.Mater.*, 2010, **9**, 205.

14 P. Jain, X. Huang, I. El-Sayed and M. El-Sayed, *Plasmonics*, 2007, **2**, 107.

15 S. Zou and G. C. Schatz, *Chem. Phys. Lett.*, 2005, **403**, 62.

16 A. Kinkhabwala, Z. Yu, S. Fan, Y. Avlasevich, K. Mullen and W. E. Moerner, *Nature*, 2008, **453**, 757.

17 K. Seungchul, J. Jonghan, K. Young-Jin, P. In-Yong, K. Yunseok and K. Seung-Woo, *Nat.Photon.*, 2009, **3**, 654.

18 A. N. Grigorenko, N. W. Roberts, M. R. Dickinson and Y. Zhang, *Nat.Photon.*, 2008, **2**, 365.

19 M. Xiao, C. Zhao, H. Chen, B. Yang and J. Wang, *Adv. Funct. Mat.*, 2012, **22**, 4526.

20 S. Camelio, D. Babonneau, D. Lantiat and L. Simonot, *Europhys. Lett.*, 2007, **79**, 47002.

21 T. Oates, A. Keller, S. Facsko and A. Mcklich, *Plasmonics*, 2007, **2**, 47.

22 I. V. Shvets, H. C. Wu, V. Usov, F. Cuccureddu, S. K. Arora and S. Murphy, *Appl. Phys.Lett.*, 2008, **92**, 023107.

23 R. Verre, K. Fleischer, R. G. S. Sofin, N. McAlinden, J. F. McGilp and I. V. Shvets, *Phys. Rev. B*, 2011, **83**, 125432.

24 R. Verre, K. Fleischer, J. F. McGilp, D. Fox, G. Behan, H. Zhang and I. V. Shvets, *Nanotech.*, 2012, **23**, 035606.

25 M. J. Brett and M. M. Hawkeye, *Science*, 2008, **319**, 1192.

26 K. Robbie and M. Brett, *J. Vac. Sci. Techn. A*, 1997, **15**, 1460.

27 R. Verre, K. Fleischer, O. Ualibek and I. V. Shvets, *Appl.Phys. Lett.*, 2012, **100**, 031102.

28 R. Lazzari and J. Jupille, *Nanotech.*, 2011, **22**, 445703.
29 P. Politi, G. Grenet, A. Marty, A. Ponchet and J. Villain, *Phys. Rep.*, 2000, **324**, 271.
30 J. M. Caridad, D. McCloskey, F. Rossella, V. Bellani, J. F. Donegan and V. Krstic, *submitted*, 2012.
31 P. C. Wu, M. Losurdo, T.-H. Kim, S. Choi, G. Bruno and A. S. Brown, *J. Vac. Sci. Tech. B*, 2007, **25**, 1019.
32 M. Losurdo, M. Bergmair, G. Bruno, D. Cattelan, C. Cobet, A. Martino, K. Fleischer, Z. Dohcevic-Mitrovic, N. Esser, M. Galliet, R. Gajic, D. Hemzal, K. Hingerl, J. Humlicek, R. Ossikovski, Z. Popovic and O. Saxl, *J. Nanopart. Res.*, 2009, **11**, 1521–1554.
33 K. Vedam, *Thin Solid Films*, 1998, **313**, 1.
34 D. E. Aspnes and A. A. Studna, *Phys. Rev. Lett.*, 1985, **54**, 1956.
35 P. Weightman, D. S. Martin, R. J. Cole and T. Farrell, *Rep. Progr. Phys.*, 2005, **68**, 1251.
36 J. Zettler, *Prog. Cryst. Growth Charact. Mater.*, 1997, **35**, 27.
37 M. Righini, C. Girard and R. Quidant, *J. Opt. A*, 2008, **10**, 093001.
38 E. C. Garnett, W. Cai, J. J. Cha, F. Mahmood, S. T. Connor, M. Greyson Christoforo, Y. Cui, M. D. McGehee and M. L. Brongersma, *Nat. Mater.*, 2012, **11**, 241.
39 C. C.B., H. J.R. and B. M.W, *Surf. Sci.*, 1997, **370**, 168.
40 R. Verre, R. Sofin, V. Usov, K. Fleischer, D. Fox, G. Behan, H. Zhang and I. V. Shvets, *Surf. Sci.*, 2012, **606**, 1815.
41 F. Cuccureddu, V. Usov, S. Murphy, C. O. Coileain and I. V. Shvets, *Rev. Sci. Instr.*, 2008, **79**, 053907.
42 H. Hövel, S. Fritz, A. Hilger, U. Kreibig and M. Vollmer, *Phys. Rev. B*, 1993, **48**, 18178.
43 M. Valamanesh, Y. Borensztein, C. Langlois and E. Lacaze, *J. Chem. Phys. C*, 2011, **115**, 2914.
44 M. Kitayama and A. M. Glaeser, *J. Am. Cer. Soc.*, 2005, **88**, 3492.
45 R. Lazzari, S. Roux, I. Simonsen, J. Jupille, D. Bedeaux and J. Vlieger, *Phys. Rev. B*, 2002, **65**, 235424.
46 J. N. Anker, W. P. Hall, O. Lyandres, N. C. Shah, J. Zhao and R. P. Van Duyne, *Nat. Mater.*, 2008, **7**, 442.
47 T. Yamaguchi, S. Yoshida and A. Kinbara, *Thin Solid Films*, 1973, **18**, 63.
48 S. Camelio, D. Babonneau, D. Lantiat, L. Simonot and F. Pailloux, *Phys. Rev. B*, 2009, **80**, 155434.
49 R. Verre, K. Fleischer, C. Smith, N. McAlinden, J. F. McGilp and I. V. Shvets, *Phys. Rev. B*, 2011, **84**, 085440.
50 C. Bohren and D. Huffman, *Absorption and scattering of light by small particles*, Wiley, New York, 1983.
51 J. D. Jackson, *Classical electrodynamic 3rd edition*, J.Wiley, New York, 1992.
52 A. Pinchuk, A. Hilger, G. von Plessen and U. Kreibig, *Nanotech.*, 2004, **15**, 1890.
53 M. Schubert, *Phys. Rev. B*, 1996, **53**, 4265.
54 M. Schubert, T. E. Tiwald and J. A. Woollam, *Appl. Opt.*, 1999, **38**, 177.
55 A. Marnier and S. Parker, *Phys. Rev. B*, 2004, **69**, 115409.
56 C. T. Campbell, *Surf. Sci. Rep.*, 1997, **27**, 1.
57 M. M. Burns, J.-M. Fournier and J. A. Golovchenko, *Phys. Rev. Lett.*, 1989, **63**, 1233.
58 V. Garcés-Chávez, R. Quidant, P. J. Reece, G. Badenes, L. Torner and K. Dholakia, *Phys. Rev. B*, 2006, **73**, 085417.